A new approach based on the combination of complex impedance and conductivity to investigate the interaction mechanisms of raw polysaccharides in aqueous solutions

Soumia Zaim, Mohamed Monkade, Halima Rchid, Alina Violeta Ursu, Christophe Vial, Philippe Michaud, Meryem Bensemlali, Abdellatif Aarfane, Rachid Nmila, Reddad El Moznine

Materials Science for Energy Technologies 6 (2023) 343–350

Contents lists available at ScienceDirect

Materials Science for Energy Technologies

journal homepage: www.keaipublishing.com/en/journals/materials-science-for-energy-technologies

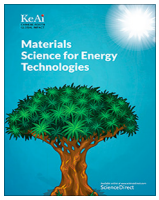

A new approach based on the combination of complex impedance and conductivity to investigate the interaction mechanisms of raw polysaccharides in aqueous solutions

Soumia Zaim [a,e,*], Mohamed Monkade [a,e], Halima Rchid [b,c,e], Alina Violeta Ursu [f], Christophe Vial [f], Philippe Michaud [f], Meryem Bensemlali [g], Abdellatif Aarfane [d,g], Rachid Nmila [b,d,e], Reddad El Moznine [a,e]

[a] Laboratoire Physique de la Matière Condensée (LPMC), Faculté des Sciences D'El Jadida, Université Chouaib Doukkali, Maroc
[b] Laboratoire Biotechnologie et Valorisation des Ressources Végétales, Faculté des Sciences D'El Jadida, Université Chouaib Doukkali, Maroc
[c] Faculté poly disciplinaire de sidi Bennour, Université Chouaib Doukkali, Maroc
[d] Ecole Supérieure d'Education et de Formation d'El Jadida, Université Chouaib Doukkali, Maroc
[e] Centre universitaire de recherche (CUR), Université Chouaib Doukkali, Maroc
[f] Université Clermont Auvergne, CNRS, SIGMA Clermont, Institut Pascal, F-63000, Clermont-Ferrand, France
[g] Laboratoire de Chimie Organique et Environnement, Faculté des Sciences D'El Jadida, Université Chouaib Doukkali, Maroc

ARTICLE INFO

Article history:
Received 1 February 2023
Revised 7 March 2023
Accepted 7 March 2023
Available online 10 March 2023

Keywords:
Polysaccharides
Interaction mechanism
Impedance
Conductivity
Equivalent circuit

ABSTRACT

The molecule-water and molecule–molecule interactions are the main keys to understanding the behavior of polysaccharides in an aqueous solution. In this work, electrical impedance spectroscopy is used to investigate raw polysaccharides' dielectric and electrical properties. Impedance data were carried out for different concentrations in the frequency range [10^{-2}–10^{6}Hz] and then analyzed in Nyquist and bode representation, revealing one clear maximum due to the electrode polarization. Therefore, the complex conductivity is analyzed and makes the other relaxation processes very clear.

Moreover, an appropriate equivalent circuit was developed, showing good agreement with the experimental data. The extrapolation and deconvolution approaches in the frequency range [10^{-3}–10^{7}Hz] were performed to confirm the presence of the three relaxation processes and the validity of the equivalent circuit. The first was attributed to the electrode polarization, and the other processes were attributed to the molecules-water and molecule-counterion interactions. Finally, a clear transition at 5% (w/v) is shown in the evolutions of the conductivity, suggesting the transition from the dilute to the semi-dilute domain.

1. Introduction

Algal hydrocolloids are essential products used in medicine, food, and industrially. Among these hydrocolloids, there are algal polysaccharides [1,2]. They have a strong affinity for water due to the presence of OH groups. These can form a hydrogen bond either with neighboring units of the same macromolecule or with neighboring chains or water molecules. Therefore, the balance between the molecule–molecule interaction and the molecule-water interaction is the key to understanding the properties of polysaccharides [3]. The dielectric properties of polyelectrolyte solutions are dominated by electrostatic interactions between the fixed charges of the polyelectrolyte and its counterions [4,5]. The electrostatic interaction is significantly related to the conformation of the polymer and the physical properties or functions of the system [6,7]. Therefore, it is crucial to investigate the dielectric and electric properties to get helpful information about the polymer conformation and the polymer/counterion interaction [8]. In this context, impedance spectroscopy has been used to study dielectric and electrical properties in an aqueous solution of raw polysaccharides.

Several works have been performed on the rheological properties of polysaccharides of algal sources [9,10,11]. Our recent work [9] found that the rheological properties exhibited interesting properties in terms of consistency and viscosity. In addition, it was found that at 5% (w/v), a net transition has occurred, suggesting the transition from the dilute to the semi-dilute solution due to the entanglement between the chain of polymers.

However, it seems that to our best knowledge, there are not enough studies on the dielectric properties of these complex systems, basically the complex conductivity. Therefore, this study was conducted in the frequency range [10^{-2}–10^{6}Hz] to investigate

* Corresponding author at: Laboratoire Physique de la Matière Condensée (LPMC), Faculté des Sciences D'El Jadida, Université Chouaib Doukkali, Maroc.
E-mail address: soumia.zaim@gmail.com (S. Zaim).

https://doi.org/10.1016/j.mset.2023.03.002
2589-2991/

the dielectric properties, especially the complex conductivity at different concentrations at room temperature.

The system's dielectric response is generally fitter by an equivalent circuit. The electrical circuit provides a simple visual model of complex time-dependent electrical and electrochemical processes by quantifying the impedance response through a combination of capacitors, resistors, and non-ideal elements [12–14]. The main advantage of modeling with electrical circuits is the analysis of different frequency spectra. However, the main challenges are finding an appropriate model to attribute physical significance to the circuit elements and modeling the frequency response of real devices with the equivalent circuit [15].

Sometimes, relaxation processes may be convoluted and/or not wholly located in the frequency range of measurement [16]. Therefore, the dielectric behavior is still being determined. In this case, extrapolation and deconvolution approaches isolate each process's contribution and identify the corresponding relaxation frequencies, such as polysaccharides. According to Einfeldt et al. and Meißner et al [17 18], the problem of the origin and interpretation of dielectric relaxations of pure polysaccharides has not been solved. In some cases, the reorientation movements of the substituent side groups frequently overlap with the local chain movement process of the pure polysaccharides, making the separation and identification of the relaxation processes more difficult. On the other hand, in the presence of water and counter-ions with the polysaccharides, the identification of the relaxation processes will be more complicated.

Two purposes are highlighted in this work. The first is low-frequency analysis for studying complex liquids, and the second is understanding the mechanism of interaction of raw polysaccharides in aqueous solutions.

In this work, a new approach was conducted to analyze the experimental data of the complex impedance and conductivity. In addition, an appropriate equivalent circuit is developed based on theoretical considerations, which showed a good fit with the experimental data. Extrapolation and deconvolution in the frequency range [10^{-3}–10^{7} Hz] were performed to investigate the relaxation process further and confirm their existence. Finally, the determination of the optimal concentration of the entanglement of the different existing elements in the solution under study.

2. Materials and methods

2.1. Extraction of raw polysaccharides

Raw polysaccharides are extracted from *Cystoreira myriophylloides* algae. Further information regarding the extraction and preparation protocol of the raw polysaccharides is given in detail in our recent work on the rheological properties [11].

2.2. Chemical composition of raw polysaccharide

2.2.1. Structural analysis

After complete hydrolysis, the raw polysaccharides were analyzed by high-performance anion-exchange chromatography (HPAEC-PAD). The procedure for Structural analysis is similar to that of Liu et al. [19]. And all chemicals used in this study were of analytical grade (purity $\geq$ 99.9%) [20]. The hydrolysis was performed in 1 mL of 2.0 M trifluoroacetic acid (TFA) in a sealed test tube at 120 °C for 1 h30. The neutralization was performed with NH4OH (35% NH_3). The precipitate was collected by centrifugation (14,000*g*/15 min). The hydrolysate was completely dissolved with ultrapure water and then fixed to 50 mL.

The analysis was performed by a Dionex ICS-3000 system that included an SP gradient pump, a pulsed amperometric detector with a gold working electrode, an Ag/AgCl reference electrode, and Chromeleon version 6.5 (Dionex Corp., Sunnyvale, CA).

2.2.2. Mineralogical analysis

Total ash contents of raw polysaccharides were determined by an inductively coupled plasma (ICP) instrument (JOBIN YVON HORIBA / Ultima 2) after calcination at 550 °C overnight.

2.3. Electrical impedance measurement

The solutions of raw polysaccharides at different concentrations (2, 3, 4, 5, 6, and 7 % (w/v)) are prepared by dissolving the dried powder in distilled water. More time is taken for stirring and allowing the solution to stand overnight to ensure thermodynamic equilibrium.

Dielectric measurements were performed using a Solartron Analytical analyzer (Materials Lab XM). The complex impedance is measured at room temperature in the frequency range [10^{-2}–10^{6}Hz]. Electrical measurements were made with a two-electrodes system. With a surface area of 1.5 cm^2, the thickness between them was 2.0 mm. The amplitude of the AC voltage applied was selected at 50 mV for all measurements based on various amplitudes using the Kramer test to maintain the system's linearity.

3. Results and discussion

3.1. Structural analysis

The analysis carried out by ion chromatography showed the existence of **fucose** (22.65%) and **galactose** (09.19%) for the monosaccharide composition and **glucuronic acid** (10.09%), with a significant proportion of the crude polysaccharides of *Cystoseira myriophylloides*. In addition, other compounds that do not exceed (5%) in composition exist, such as mannose, rhamnose, xylose, glucosamine, and xylose. The chemical composition obtained is almost similar to that of other researchers [21,22].

3.2. Analysis of mineralogical composition

The ICP analysis showed that the raw polysaccharides contain oligo-elements (monovalent cations) such as potassium (**69.15%**), sodium (**5.63%**), as well as some divalent cations such as magnesium (**15.24%**), and calcium (**6.33%**).

The ash content estimated in this study was higher than that obtained by Khajouei et al. [23]. This difference can be due to the effect of geographical location and season of algae harvesting.

3.3. Analysis of the complex impedance of raw polysaccharide at different concentrations

The dependence of the real and imaginary parts of the complex impedance as a function of frequency at different concentrations of raw polysaccharides are shown in Fig. 1 (a-b). As can be observed, all raw polysaccharide concentrations show the same frequency dependence except for the 0% concentration, which shows a very clear relaxation peak in the frequency range.

The plots of the reel and imaginary part of the complex impedance are inadequate to identify the relaxation processes and highlight the evolution of the complex impedance as a function of the concentration. In this situation, the relaxation processes could be hidden, and it was not easy to find their origins. Therefore, it would be difficult to identify this sample's relaxation times and frequencies.

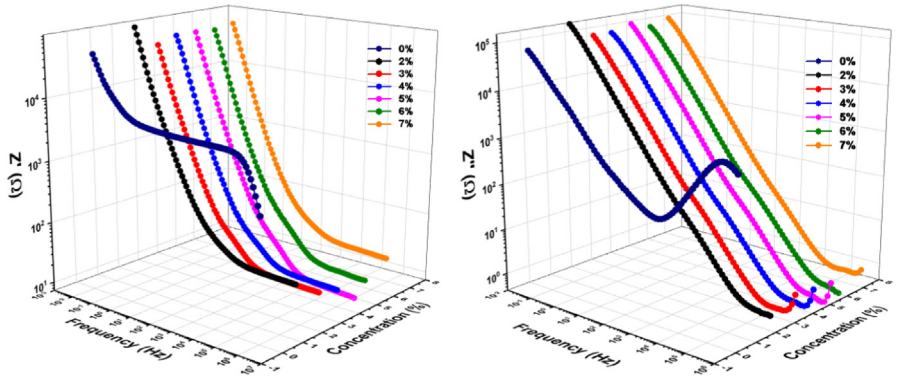

Fig. 1. Real (a) and Imaginary (b) parts of the complex impedance as a function of the frequency of raw polysaccharides at different concentrations.

To give a background to our following discussion and analysis of impedance data, we give so far only a summary. It is well known that different forms of dielectric response are commonly observed in a complex sample like polyelectrolyte. The electrode polarization cannot be avoided [24]. Either the bulk has an electrical impedance so that the applied voltage drops quasi-uniformly throughout the thickness of the sample, or the bulk impedance is lower than that present in the region of the electrodes. In the former case, one can describe the response in terms of the bulk properties of the material, while in the latter case, the response is dominated by charge accumulation near the electrodes leading to the formation of barrier layers that are formed at the electrode surface. Therefore, this behavior could analyze the impedance data very complicated and how to isolate the contribution of electrode polarization.

According to the analysis of the composition, it is found that the sample can be considered an ionic polysaccharide. In this case, the electrical properties of the solution are considered to be dominated by the electrostatic interactions among the fixed charges on the polyelectrolyte and its counterions. The electrostatic interaction is significantly related to polymer conformation and physical properties. The counterions can be classified into two groups, the tightly bound counterions, and the loose ones. For divalent cations such as magnesium (**15.24%**) and calcium (**6.33%**), strong interactions are expected with these later cations and carboxyl groups on adjacent polymer chains since the chemical composition showed their existence. As for monovalent cations such as potassium (**69.15%**) and sodium (**5.63%**), these cations are expected to make hopping movements between the polymer chains of the monosaccharides. Some of them can move up to the electrodes. Therefore, we can suspect the contributions of electrode polarization in the low-frequency region.

The mobility and the fluctuations of the tightly bound counterions can occur within a short range of the length fluctuations and, therefore, a short time. In contrast, the mobility of the loosely bound counterions can occur within an extended range of the length via hopping from the neighboring site. Therefore, the contributions of the tightly bound counterions are expected to be seen in the high-frequency region, and the contributions of the loosely bound counterions are expected to be seen in the low-frequency region [8]. Based on all these considerations, we focused on the complex conductivity analysis in the next section.

Since all raw polysaccharide concentrations showed the same frequency dependence, the concentration of 5% (w/v) will be selected for an in-depth analysis of this behavior as a function of frequency.

3.3.1. Modeling of the impedance data with an equivalent circuit

The analysis of other authors on the dielectric behavior of polysaccharides in aqueous solutions showed the existence of two relaxation processes, the first around 1 kHz, and the second appearing at frequencies above 1 MHz [5]. For these reasons, the equivalent circuit (Fig. 2) developed for analyzing the impedance data will be composed of three parts, and each part will be attributed to a specific relaxation. Therefore, the equivalent circuit could reflect the electrical behavior of three types of relaxations.

Fig. 3 shows the modeling results with the equivalent circuit developed to analyze the impedance data of the concentration 5% (w/v).

The modeling with the equivalent circuit agrees well with the experimental data in the studied frequency range. For this reason, it is vital to calculate the expression of the complex impedance of the equivalent circuit developed to obtain each relaxation frequency.

The expression of the impedance can be written as follow:

$$Z*(\omega) = R_s + \frac{R_1}{1+(j\omega\tau_{z1})^{p_1}} + \frac{R_2}{1+(j\omega\tau_{z2})^{p_2}} + \frac{R_3}{1+(j\omega\tau_{z3})^{p_3}} \quad (1)$$

With

$$\tau_{z_i} = (R_i.T_i)^{1/p_i} \quad i = 1,2,3 \quad (2)$$

where $\tau_{zi,}$ are the relaxation times.

Each term in the above expression (1) is similar to the Cole-Cole relaxation parameters in the complex permittivity [24]:

$$\varepsilon^*(\omega) = \varepsilon_\infty + \frac{\Delta\varepsilon}{1+(i\omega\tau_\varepsilon)^p} \quad (4)$$

where ε_s and ε_∞ are the low and high-frequency dielectric constants values, respectively, τ_ε is the relaxation time, $\Delta\varepsilon$ is the dielectric strength ($\Delta\varepsilon$ = ε_s-ε_∞), and p is an exponent between 0 and 1.

The presence of a maximum in the evolution of the imaginary part of the complex permittivity as a function of frequency characterizes this relaxation process. This maximum is localized at:

$$w_{\max} = \frac{1}{\tau_{z_1}} = \frac{1}{(R_1.T_1)^{1/p_1}} \quad (5)$$

Therefore, this behavior can be rewritten as follows:

$$Z^*(\omega) = Z_\infty + \frac{\Delta Z}{1+(i\omega\tau_z)^p} \quad (6)$$

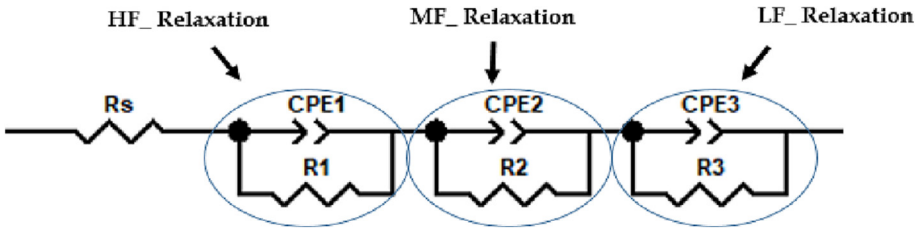

Fig. 2. Equivalent circuit developed to fit experimental data of impedance spectrum and complex conductivity at different concentrations.

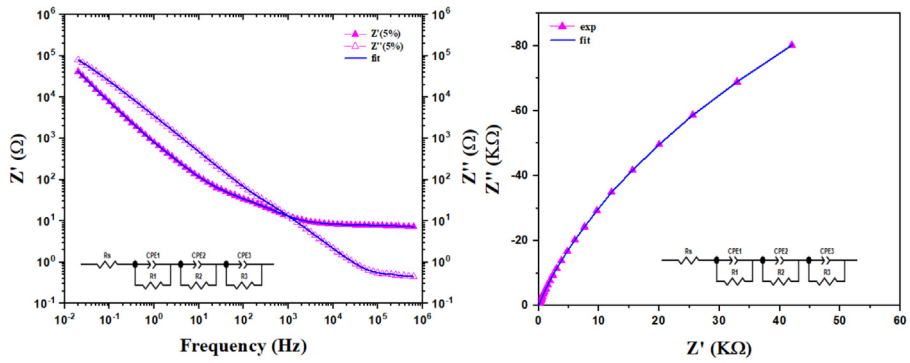

(a) (b)

Fig. 3. Evolution of the real (a) and imaginary (b) part of the impedance as a function of frequency for 5% (w/v) of raw polysaccharides.

where $\tau_z=(2\pi f)^{-1}$ is the relaxation time and $\Delta Z = Z_\infty - Z_s$ is the interrelated dielectric increments, and Z_∞ and Z_s are the values of the impedance at high and low frequencies [25].

The obtained parameters of the equivalent circuit are shown in Table 1 at different concentrations.

Table 1 shows a clear transition of all parameters at 5% (w/v) of concentration. For example, the relaxation frequencies of each process of the concentration of 5% (w/v) are f_1 = 5,59 × 10^{-3}Hz, f_2 = 4.89 × 10^{2}Hz, and f_3 = 6.96 × 10^{5}Hz. Therefore, for better visualization of these relaxation processes, an extrapolation of the impedance data in the frequency range [10^{-3}-10^{7}Hz] will be used.

3.3.2. Extrapolation and deconvolution of the impedance data of each process.

The extrapolation and deconvolution approach, in the frequency range [10^{-3}-10^{7}Hz], were performed to follow the impedance trend and highlight the relaxation processes. The equivalent circuit developed corresponds to three types of Cole-Cole relaxation.

According to Fig. 4 (a), it can be seen that the deconvolution approach can identify each process and then extract the relaxation time corresponding to the maximum of each peak. The imaginary part of the impedance thus reveals three relaxation maxima, approximately at a low frequency, around 0.01 Hz, the second relaxation peak between 10^2 and 10^3Hz, and the last at a high frequency of 1.05 × 10^6Hz.

The Nyquist representation (Fig. 4 (b)) shows a single semicircle. However, the inset shows the existence of two semicircles dominated by low-frequency electrode polarization.

As mentioned previously, complex conductivity is beneficial for analyzing dielectric properties. In addition, impedance measurements could be relatively slow to observe mobility and relaxation processes.

3.4. Analysis of the complex conductivity

The complex conductivity σ^* (ω) can be obtained from the expression of the complex impedance according to the following relationship [26,27]:

$$\sigma*(\omega) = k \times \frac{1}{Z*(\omega)} \tag{11}$$

where k is the cell constant.

According to this relationship, any process hidden in the impedance plot is expected to be more amplified in the conductivity evolution.

Our study uses the complex conductivity of the raw polysaccharides for different concentrations. It was obtained using ZView

Table 1
Parameters from the fitting with the equivalent circuit for the raw polysaccharides at different concentrations.

C (%)	Rs (Ω)	$CPE_1\_T_1$ (μF)	$CPE_1\_p_1$	R_1 (Ω)	$CPE_2\_T_2$ (μF)	$CPE_2\_p_2$	R_2 (Ω)	$CPE_3\_T_3$ (μF)	$CPE_3\_p_3$	R_3 (MΩ)
2	16,76	010,0	0,77	1,45	065,38	0,90	18,68	58,39	0,85	0,27
3	12,99	050,0	0,63	1,67	070,98	0,88	13,78	62,56	0,86	0,19
4	8,78	145,8	0,56	1,61	122,84	0,82	21,34	68,87	0,87	0,18
5	**6,47**	**100,0**	**0,57**	**1,64**	**065,69**	**0,89**	**11,99**	**57,55**	**0,87**	**0,32**
6	17,82	003,2	0,90	1,18	267,60	0,74	13,89	57,95	0,88	0,26
7	31,69	005,0	0,82	2,98	174,89	0,75	26,55	50,51	0,89	0,15

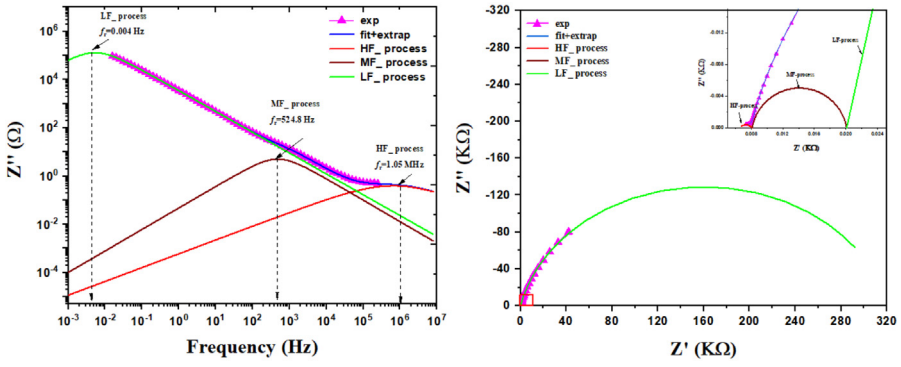

Fig. 4. Bode (a) and Nyquist diagrams in the frequency range [10^{-3}–10^{7}Hz].

software, and its evolution according to each concentration is shown in Fig. 5.

Fig. 5(a) shows that all concentrations have the same frequency dependence except distilled water. Compared to the evolution of the plots of the imaginary part of the complex impedance, the imaginary part σ"(ω) showed a vast peak, which suggests the convolution of several processes and the beginning of the appearance of another process in the high-frequency region (Fig. 6).

It is important to note that the magnitude of these peaks increases with increasing concentration up to 5% of raw polysaccharide concentration. Then the magnitude started to decrease. In addition, the frequency corresponding to these peaks shifts to the high frequency up to 5%, then shifts to the low-frequency region. These behaviors were not seen in the plots of the impedance versus the frequency.

Regarding the Nyquist plot (Fig. 5-b), the evolutions also showed a depressed semicircle and the beginning of the appearance of another high-frequency process. On the other hand, from the inset in the Nyquist diagram, the distilled water reveals a relaxation peak and a straight line in the imaginary part of the conductivity. The inset in the Nyquist diagram clearly shows a semicircle and a straight line.

A clear distinction between the different concentrations is shown in both concentration regions. In the first concentration region (below 5% (w/v)), the diameter of the semicircle increases with the concentration. This behavior is reflected by an increase in the counterion charges in the solution and the phenomenon of diffusion between the particles. In contrast, in the second region (above 5% (w/v)), the diameter of the semicircles decreases with the concentration increase. This behavior decreases the counterion charges in the solution due to the entanglement of the different components of the solution.

3.4.1. Modeling of the complex conductivity

Fig. 6 (a-b) shows the Bode and Nyquist plots of the complex conductivity of the selected concentration 5% (w/v) in the frequency range [10^{-2}-10^{6}Hz].

More interesting, the developed equivalent electrical circuit to fit the impedance data perfectly fit the experimental data of the complex conductivity. These results confirm the validity of this circuit developed for analyzing the experimental data.

As was observed from impedance data, the extrapolation approach confirms the existence of the third relaxation process at high frequency. Therefore, it seems very important to follow the same approach to highlight the existence of three relaxation processes.

The electrical circuit used to model the impedance data and complex conductivity is only a superposition of three Randles-type circuits, characteristic of a Cole-Cole relaxation. Due to simplifying the theoretical calculation of the complex conductivity, one block of the circuit is considered to calculate the expression of the relaxation time.

The expression of the complex conductivity is:

$$\sigma^*(\omega) = k \times \frac{\left[(R_{s_i}+R_i)+(2R_{s_i}+R_i)\tau_i^{p_i}\omega^{p_i}\cos(p_i\pi/2)+R_{s_i}\tau_i^{2p_i}\omega^{2p_i}\right]+j\left[R_i\tau_i^{p_i}\omega^{p_i}\sin(p_i\pi/2)\right]}{(R_{s_i}+R_i)^2+2(R_{s_i}+R_i)R_{s_i}\tau_i^{p_i}\omega^{p_i}\cos(p_i\pi/2)+R_{s_i}^{2p_i}\tau_i^{2p_i}\omega^{2p_i}}$$

This expression is similar to that representing the Cole-Cole relaxation in the complex permittivity [25]:

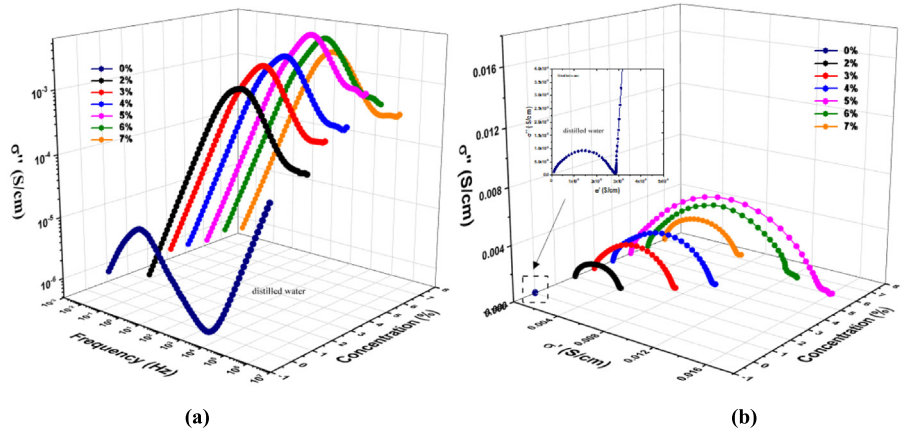

Fig. 5. Bode (a) and Nyquist (b) plots of complex conductivity spectra of raw polysaccharides at different concentrations.

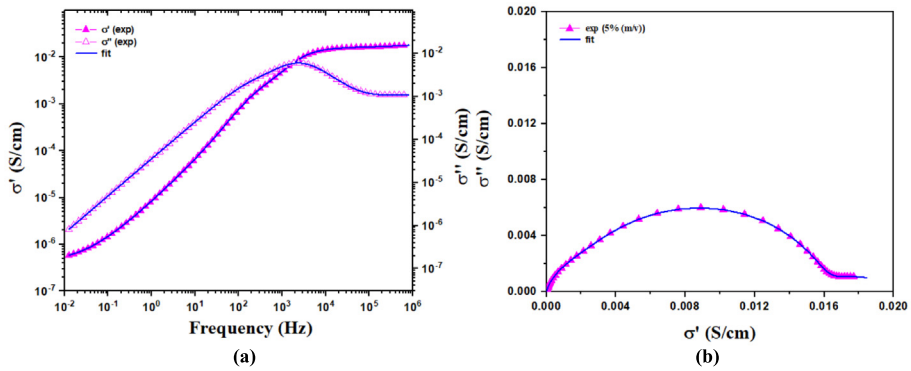

Fig. 6. Bode (a) and Nyquist (b) diagrams of the complex conductivity.

$$\varepsilon^*(\omega) = \varepsilon_\infty + \frac{\Delta\varepsilon}{1 + (i\omega\tau_\varepsilon)^p} \tag{15}$$

where ε_s and ε_∞ are the low-frequency and the high-frequency dielectric constants values, respectively, τ is the relaxation time, $\Delta\varepsilon$ is the dielectric strength ($\Delta\varepsilon = \varepsilon_s - \varepsilon_\infty$), and p is an exponent between 0 and 1.

In this case, this behavior can be described by the following equations:

$$\sigma^*(\omega) = \sigma_\infty + \frac{\Delta\sigma}{1 + (i\omega\tau_\sigma)^p} \tag{16}$$

where $\tau_\sigma=(2\pi f)^{-1}$ is the relaxation time and $\Delta\sigma = \sigma_\infty$-$\sigma_s$ is the interrelated dielectric increments, σ_∞ and σ_s are the values of the conductivity at high and low frequencies, respectively [25].

The following expression describes the evolution of the complex conductivity (equation (12):

$$\sigma^*(\omega) = \sigma_{\infty HF} + \frac{\Delta\sigma_{HF}}{1 + (i\omega\tau_{\sigma HF})^{p_1}} + \sigma_{\infty MF} + \frac{\Delta\sigma_{MF}}{1 + (i\omega\tau_{\sigma MF})^{p_2}} + \sigma_{\infty LF} + \frac{\Delta\sigma_{LF}}{1 + (i\omega\tau_{\sigma LF})^{p_3}} \tag{21}$$

According to this formula, the global expression of the complex conductivity can be expressed by a superposition of three Cole-Cole relaxation processes: at high, medium, and low frequencies.

For example, the relaxation frequencies of each process of the concentration 5% are $f_{\sigma1}$ = 0.41 × 10^3Hz, $f_{\sigma2}$ = 1.33 × 10^3Hz, and $f_{\sigma3}$ = 0.26 × 10^6Hz. Therefore, for better visualization of these relaxation processes, an extrapolation of the conductivity data in the frequency range [10^{-2}-10^7Hz] will be used.

3.4.2. Extrapolation and deconvolution approaches of each relaxation process of the conductivity

The extrapolation in the frequency range [10^{-2}–10^7Hz] was performed to investigate the trends of the conductivity. In addition, the separation and deconvolution of all processes were performed to analyze each relaxation process (Fig. 7).

The imaginary part of the complex conductivity shows a very broad relaxation peak, indicating the existence of two convoluted peaks around 114.82 and 2389.8 Hz. Moreover, another peak appears at a high frequency of 1.73 MHz above 1 MHz. Similarly, the extrapolation in this frequency range is very useful in highlighting these relaxation processes. Moreover, the Nyquist representation shows a very broad semicircle and a high-frequency semicircle corresponding to the high-frequency process.

In the same way, to analyze the different relaxation processes, the deconvolution approach will be used to analyze each process. The imaginary part of the complex conductivity reveals three relaxation peaks at a low frequency of around 316 Hz, the second relaxation peak at 1122 Hz, and the last at a high frequency (1.05 × 10^6 Hz). In addition, the Nyquist representation shows three semicircles corresponding to the relaxations at low, medium, and high frequencies. From this figure, all processes are visible in the studied frequency range and are not dominated by electrode polarization.

3.5. Origin of the different relaxation processes

At this stage, three relaxations have been identified. Therefore, it is essential to define their origins. The identification by ion chromatography revealed the existence of different anionic monosac-

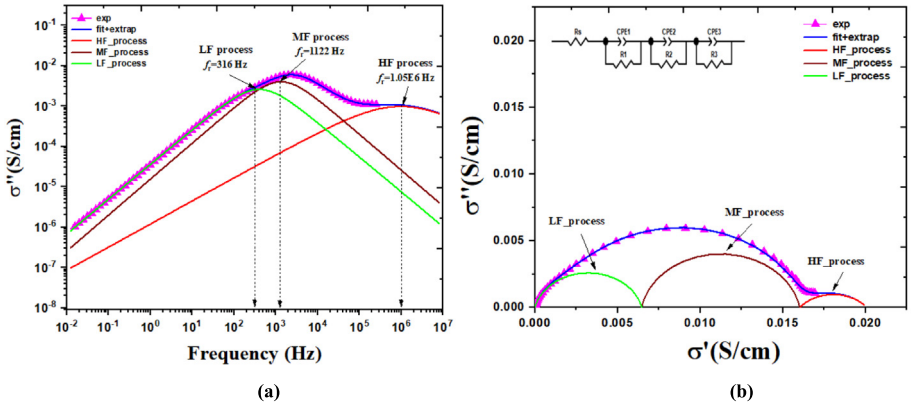

Fig. 7. Bode (a) and Nyquist (b) representations of the 5% polysaccharide concentration. The solid line corresponds to the fit and extrapolation in the frequency range [10^{-2}–10^7Hz].

charides. In addition, the ICP showed the presence of 30% of mineral elements, which will play the role of counterions. We expect only one ionic species to contribute to the conduction process for a dissociating material with several conductive fractions, anionic monosaccharides, and cationic mineral elements.

The first process at a medium frequency could be attributed to the electrostatic interactions of the counter ions, which are very strongly bound to the anions (negative sites) of each component of the sample polysaccharide under investigation since these latter are considered to be anionic polymers. The second process can be attributed to the counter ions' electrostatic interactions, which are very slightly bound to the polysaccharide anions without forgetting the protons (H^+) and the hydroxyl group (OH^-) coming from the water. Therefore, these two relaxation processes can reflect the nature of the cohesive force between the counterions and the negative sites of each constituent of the polysaccharides [5]. These two relaxations were translated by two different relaxation times, which means that the first process at high frequency occurred in a short time while the second scale at medium frequency occurred in a long-time scale. Moreover, at low frequencies, the polarization of the electrode could be due to the accumulation of free ions on the electrode surfaces [28].

4. Conclusion

In this study, the effect of the concentration of raw polysaccharides on the dielectric properties is investigated. Impedance and conductivity data were analyzed and fitted with an appropriate equivalent circuit which showed a good agreement with the experimental data. Moreover, the extrapolation of the data in the frequency range [10^{-3}-10^{7}Hz] is carried out to investigate the relaxation processes, especially the high-frequency relaxation process above 1 MHz. The deconvolution approach is used to identify the conduction processes. Consequently, three relaxation processes are identified in Bode and Nyquist diagrams of complex conductivity evolution. This evolution shows a clear transition at 5%(w/v), suggesting the transition from the dilute to the semi-dilute domain. These results showed a good correlation with our recent work related to the study carried out on rheological properties [9]. Finally, our approach is an effective method for analyzing the distribution of polymer chains and the nature of counterions binding in polysaccharide solutions.

CRediT authorship contribution statement

Soumia Zaim: Conceptualization, Methodology, Investigation, Software, Data curation, Writing – original draft, Visualization. **Mohamed Monkade:** Investigation, Supervision, Funding acquisition. **Halima Rchid:** Investigation, Supervision, Project administration, Funding acquisition. **Alina Violeta Ursu:** Investigation, Supervision, Project administration, Funding acquisition. **Christophe Vial:** Investigation, Supervision, Project administration, Funding acquisition. **Philippe Michaud:** Investigation, Supervision, Project administration, Funding acquisition. **Meryem Bensemlali:** Data curation, Writing – review & editing, Visualization. **Abdellatif Aarfane:** Data curation, Writing – review & editing, Visualization. **Rachid Nmila:** Supervision, Project administration, Funding acquisition. **Reddad El Moznine:** Supervision, Project administration, Funding acquisition.

Declaration of Competing Interest

The authors declare that they have no known competing financial interests or personal relationships that could have appeared to influence the work reported in this paper.

References

[1] N. Wei, J. Quarterman, Y.-S. Jin, Marine macroalgae: an untapped resource for producing fuels and chemicals, Trends Biotechnol. 31 (2013) 70–77, https://doi.org/10.1016/j.tibtech.2012.10.009.

[2] I. Wijesekara, W.K.D.S. Karunarathna, Chapter 18 - Usage of Seaweed Polysaccharides as Nutraceuticals, in: J. Venkatesan, S. Anil, S.-K. Kim (Eds.), Seaweed Polysaccharides, Elsevier, 2017: pp. 341–348. https://doi.org/10.1016/B978-0-12-809816-5.00018-9.

[3] M.Q. Guo, X. Hu, C. Wang, L. Ai, Polysaccharides: Structure and Solubility, IntechOpen, 2017, 10.5772/intechopen.71570.

[4] J.-H. Yoon, Y.A. Kumar, S. Sambasivam, S.A. Hira, T.N.V. Krishna, K. Zeb, W. Uddin, K.D. Kumar, I.M. Obaidat, S. Kim, H.-J. Kim, Highly efficient copper-cobalt sulfide nano-reeds array with simplistic fabrication strategy for battery-type supercapacitors, J. Storage Mater. 32 (2020), https://doi.org/10.1016/j.est.2020.101988 101988.

[5] E. Prokhorov, G. Luna-Barcenas, S. Kumar-Krishnan, R.A. Mauricio Sánchez, B.E. Castillo Reyes, J. Hernández Vargas, Probing molecular interactions of polysaccharides in the presence of water, J. Mol. Struct. 1218 (2020), https://doi.org/10.1016/j.molstruc.2020.128531 128531.

[6] Y.A. Kumar, G. Mani, M.R. Pallavolu, S. Sambasivam, R.R. Nallapureddy, M. Selvaraj, M. Alfakeer, A.A.A. Bahajjaj, M. Ouladsmane, S.S. Rao, S. Ramakrishna, Facile synthesis of efficient construction of tungsten disulfide/iron cobaltite nanocomposite grown on nickel foam as a battery-type energy material for electrochemical supercapacitors with superior performance, J. Colloid Interface Sci. 609 (2022) 434–446, https://doi.org/10.1016/j.jcis.2021.11.193.

[7] C. Roldan-Cruz, J. Carmona-Ascencio, E.J. Vernon-Carter, J. Alvarez-Ramirez, Electrical impedance spectroscopy for monitoring the gum Arabic–chitosan complexation process in bulk solution A Physicochemical and engineering aspects, (2016). https://pubag.nal.usda.gov/catalog/5529402 (accessed July 31, 2021).

[8] S. Ikeda, H. Kumagai, K. Nakamura, Dielectric analysis of food polysaccharides in aqueous solution, Carbohydr. Res. 301 (1997) 51–59, https://doi.org/10.1016/S0008-6215(97)00082-7.

[9] S. Zaim, O. Cherkaoui, H. Rchid, R. Nmila, R. El Moznine, Rheological investigations of water-soluble polysaccharides extracted from Moroccan seaweed Cystoseira myriophylloides algae, Polymers Renewable Resour. 11 (2020) 49–63, https://doi.org/10.1177/2041247920960956.

[10] F. Hentati, G. Pierre, A.V. Ursu, C. Vial, C. Delattre, S. Abdelkafi, P. Michaud, Rheological investigations of water-soluble polysaccharides from the Tunisian brown seaweed Cystoseira compressa, Food Hydrocoll. 103 (2020), https://doi.org/10.1016/j.foodhyd.2019.105631 105631.

[11] S. Zaim, A. Mortadi, F. Chibi, E.H. Benchennouf, W. Arsalane, O. Cherkaoui, H. Rchid, R. Nmila, R. El Moznine, Extraction of polysaccharides from brown algae: rheological studies, Iran, Polym. J. 29 (2020) 1137–1145, https://doi.org/10.1007/s13726-020-00867-9.

[12] M. Moniruzzaman, Y. Anil Kumar, M.R. Pallavolu, H.M. Arbi, S. Alzahmi, I.M. Obaidat, Two-dimensional core-shell structure of cobalt-doped@MnO2 nanosheets grown on nickel foam as a binder-free battery-type electrode for supercapacitor application, Nanomaterials 12 (2022) 3187, https://doi.org/10.3390/nano12183187.

[13] Y.A. Kumar, H.-J. Kim, Effect of time on a hierarchical corn skeleton-like composite of CoO@ZnO as capacitive electrode material for high specific performance supercapacitors, Energies 11 (2018) 3285, https://doi.org/10.3390/en11123285.

[14] E. von Hauff, Impedance spectroscopy for emerging photovoltaics, J. Phys. Chem. C 123 (18) (2019) 11329–11346.

[15] D. Harrington, P. Driessche, Mechanism and equivalent circuits in electrochemical impedance spectroscopy, Electrochim. Acta 56 (2011) 8005–8013, https://doi.org/10.1016/j.electacta.2011.01.067.

[16] M. Chahbi, A. Mortadi, S. Zaim, N. El Ghyati, M. Monkade, R. El Moznine, A new approach to investigate the ionic conductivity of NaCl and KCl solutions via impedance spectroscopy, Mater. Today:. Proc. 66 (2022) 205–211.

[17] J. Einfeldt, D. Meißner, A. Kwasniewski, Contributions to the molecular origin of the dielectric relaxation processes in polysaccharides – the high temperature range, J. Non Cryst. Solids 320 (2003) 40–55, https://doi.org/10.1016/S0022-3093(03)00086-3.

[18] D. Meißner, J. Einfeldt, A. Kwasniewski, Contributions to the molecular origin of the dielectric relaxation processes in polysaccharides – the low temperature range, J. Non Cryst. Solids 275 (2000) 199–209, https://doi.org/10.1016/S0022-3093(00)00248-9.

[19] L. Liu, J. Feng, K. Gao, S. Zhou, M. Yan, C. Tang, J. Zhou, Y. Liu, J. Zhang, Influence of carbon and nitrogen sources on structural features and immunomodulatory activity of exopolysaccharides from Ganoderma lucidum, Process Biochem. 119 (2022) 96–105, https://doi.org/10.1016/j.procbio.2022.05.016.

[20] D.K. Kulurumotlakatla, A.K. Yedluri, H.-J. Kim, Hierarchical NiCo2S4 nanostructure as highly efficient electrode material for high-performance supercapacitor applications, J. Storage Mater. 31 (2020), https://doi.org/10.1016/j.est.2020.101619 101619.

[21] R. Zhang, X. Zhang, Y. Tang, J. Mao, Composition, isolation, purification and biological activities of Sargassum fusiforme polysaccharides: a review, Carbohydr. Polym. 228 (2020), https://doi.org/10.1016/j.carbpol.2019.115381 115381.

[22] P. Shao, X. Chen, P. Sun, In vitro antioxidant and antitumor activities of different sulfated polysaccharides isolated from three algae, Int. J. Biol.

Macromol. 62 (2013) 155–161, https://doi.org/10.1016/j.ijbiomac.2013.08.023.
[23] R.A. Khajouei, J. Keramat, N. Hamdami, A.-V. Ursu, C. Delattre, C. Laroche, C. Gardarin, D. Lecerf, J. Desbrières, G. Djelveh, P. Michaud, Extraction and characterization of an alginate from the Iranian brown seaweed Nizimuddinia zanardini, Int. J. Biol. Macromol. 118 (2018) 1073–1081, https://doi.org/10.1016/j.ijbiomac.2018.06.154.
[24] A. Mortadi, A. Elmelouky, E.G. Chahid, R. Essajai, H. Naserllah, M. Chahbi, N. Ghyati, S. Zaim, O. Cherkaoui, R. El Moznine, Effects of calcium oxide on the surface properties of industrial sludge by analyzing rheological and electrical properties, J. Environ. Chem. Eng. 8 (3) (2020) 103764.
[25] M. Esch, V.L. Sukhorukov, M. Kürschner, U. Zimmermann, Dielectric properties of alginate beads and bound water relaxation studied by electrorotation, Biopolymers 50 (1999) 227–237, https://doi.org/10.1002/(SICI)1097-0282(199909)50:3<227::AID-BIP1>3.0.CO;2-Y.
[26] R.V. Barde, K.R. Nemade, S.A. Waghuley, Impedance spectroscopy study of the AC conductivity of sodium superoxide nanoparticles doped vanadate based glasses, Mater. Sci. Energy Technol. 4 (2021) 202–207, https://doi.org/10.1016/j.mset.2021.06.004.
[27] A. Mortadi, E.G. Chahid, A. Elmelouky, M. Chahbi, N. EL Ghyati, S. Zaim, O. Cherkaoui, R. El Moznine, Complex electrical conductivity as a new technique to monitor the coagulation-flocculation processes in the wastewater treatment of the textile Industry, Water Resour. Ind. 24 (2020), https://doi.org/10.1016/j.wri.2020.100130 100130.
[28] Madhusudhana, G. Manasa, A.K. Bhakta, Z. Mekhalif, R.J. Mascarenhas, Bismuth-nanoparticles decorated multi-wall-carbon-nanotubes cast-coated on carbon paste electrode; an electrochemical sensor for sensitive determination of Gallic Acid at neutral pH, Mater. Sci. Energy Technol. 3 (2020) 174–182.